Automatic detection of solar active regions from SOHO/MDI and SDO/HMI synoptic magnetograms

Ruihui Wang（wangruihui@buaa.edu.cn）, Jie Jiang（jiejiang@buaa.edu.cn）, Yukun Luo
School of Space and Environment, Beihang University, China

Abstract

Aim:

1. Develop a new method to automatically detect ARs from SOHO/MDI and SDO/HMI radial synoptic magnetograms;
2. Provide a new homogenous database of ARs between 1996 and 2020.

Methods:

1. Morphological operation and region growing for the detection of ARs;
2. Calibration between HMI and MDI data based on identified ARs flux and area to generate the homogenous ARs dataset.

Results:

1. We develop an adaptive method to automatically identify ARs from synoptic maps observed by different instruments, and further derive a homogenous dataset including ARs' area and flux over the last two solar cycles. The validation of the method is demonstrated by Figs. 2 and 4. The data are compared with other datasets, which show reasonable agreement (See Fig. 5).
2. The identified ARs during the overlap period of MDI and HMI have the same areas as a whole. The identified AR flux based on MDI maps is about 1.36 times as large as that of HMI maps (See Fig. 3).
3. Strong ARs (|flux| > 10^{22}Mx) contribute most to the difference between cycles 23 and 24. Other ARs (|flux| < 10^{22}Mx) are similar in the two cycles in both area and flux (See Fig. 6).

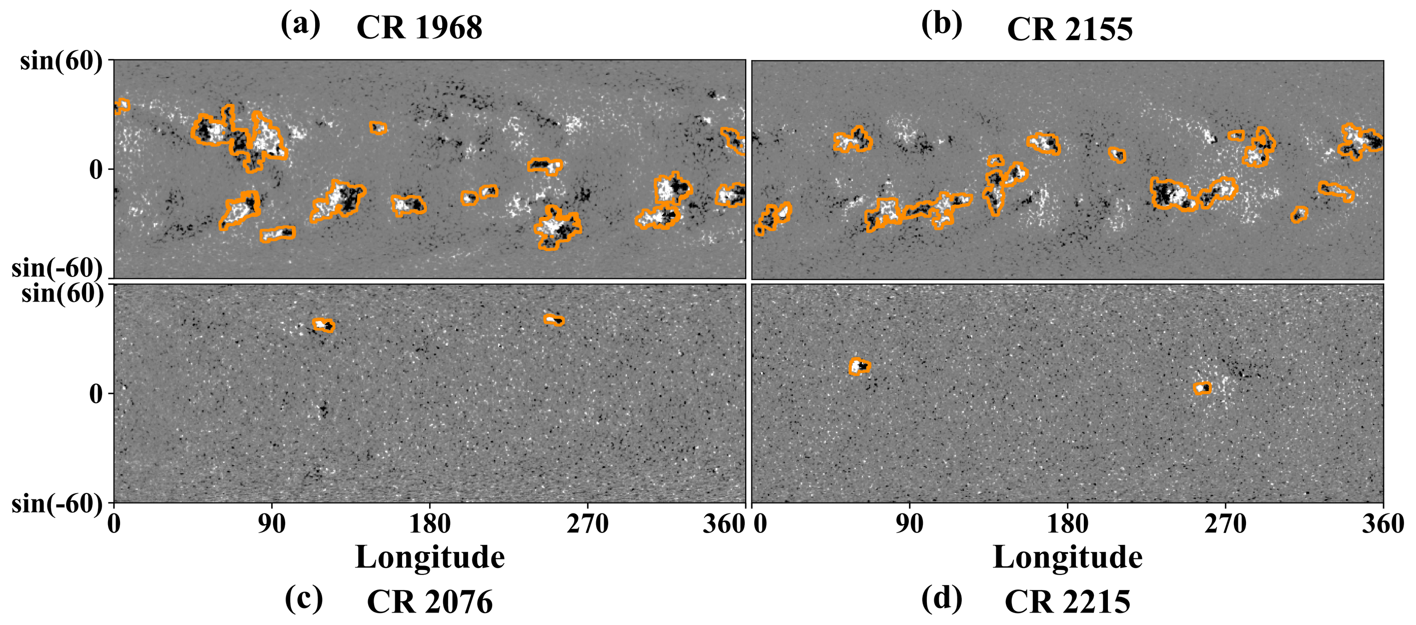

Fig. 2. Examples of the detected ARs based on synoptic magnetograms. MDI (left) and HMI (right) at different phases of cycles 23 and 24 are used to demonstrate the accuracy of the algorithm. The 4 magnetograms are overplotted with the contours in dark orange outlining the perimeter of the detected ARs.

Acknowledgements The SDO/HMI data are courtesy of NASA and the SDO/HMI team. SOHO is a project of international cooperation between ESA and NASA. The research is supported through the National Natural Science Foundation of China (grant Nos. 12173005 and 11873023).

Reference

[1] A. Munoz-Jaramillo, et al. 2016, IEEE International Conference on Big Data, 3194
[2] Monica G. Bobra, et al. 2021, APJS. 256,26
[3] Monica G. Bobra, et al. 2014, Sol Phys. 289, 3549–3578.
[4] USAF/NOAA data: http://solarcyclescience.com/activeregions.html

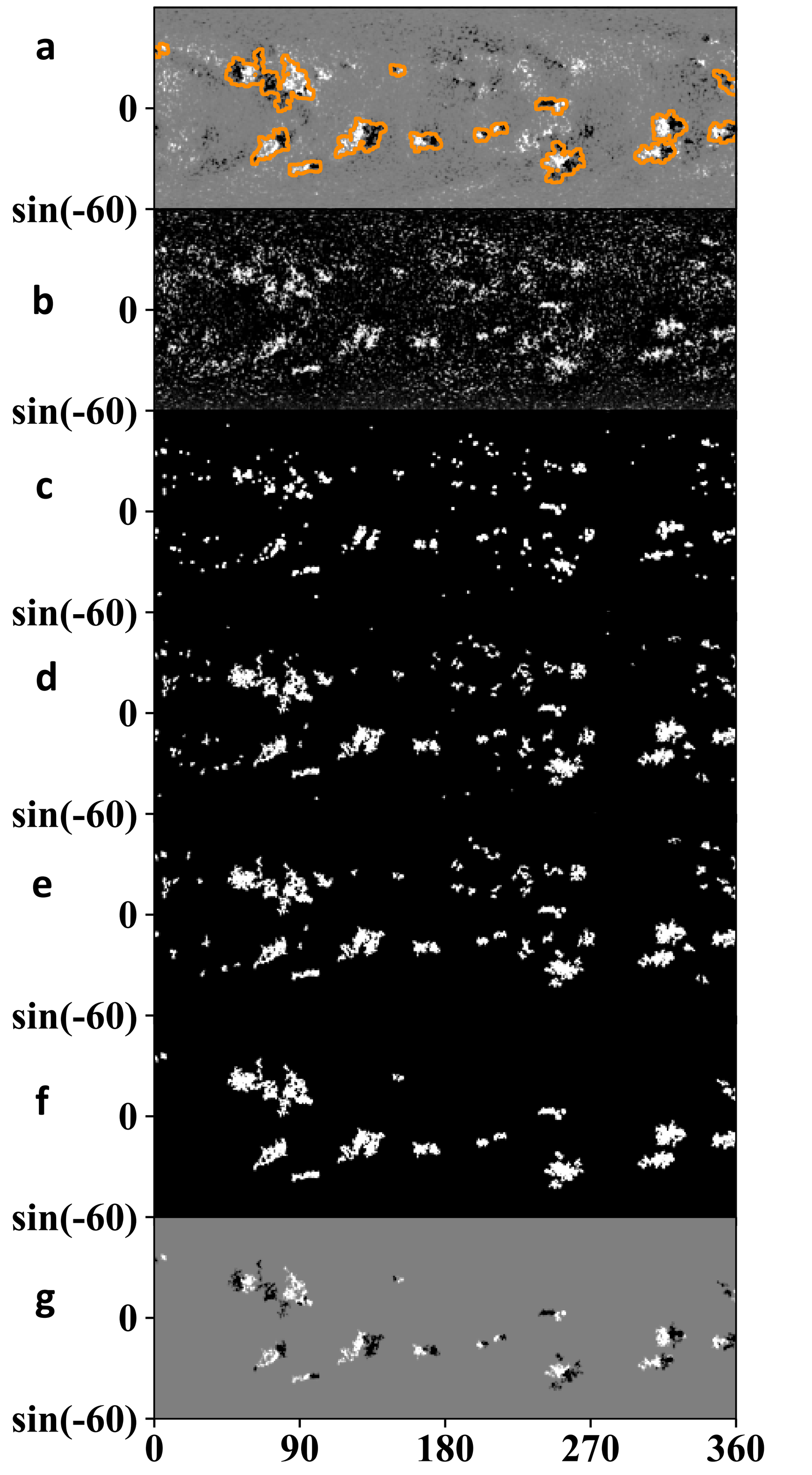

Fig.1. Illustration of the AR detection algorithm. The synoptic map of CR 1968 is used as an example.

Method

Table1. Parameters in the detection method

Module	Controlling Parameter	Value	Acceptable Parameter Ranges
(1)	Gaussian smoothing kernel (kernel1)	501 pixels	[101-1001] pixels
	Constant C	10 G	[5-15] G
(2)	closing operation kernel (kernel2)	3 pixels	[3-5] pixels
	opening operation kernel (kernel3)	MDI:11 pixels	[9-13] pixels
		HMI: 9 pixels	[7-11] pixels
(3)	threshold	MDI: 50 G	fixed values based on literatures
		HMI: 30 G	
(4)	closing operation kernel(kernel4)	5 pixels	[3-7] pixels
	area threshold	351 pixels $\approx$ 412 Mm^2	fixed values based on the ARs size
(5)	dilation operation kernel(kernel5)	23 pixels	[15-31] pixels
	threshold of flux imbalance($\frac{\lvert F_+ + F_- \rvert}{\lvert F_+\rvert + \lvert F_-\rvert}$)	0.5	[0.4-0.8]

- ➢ Latitude range of detection: ±60°
- ➢ Five modules (see Fig. 1 and below) in the detection algorithm. Parameters and their acceptable ranges are listed in Table 1.

• Fig. 1b, adaptive threshold segmentation to remove the background magnetic fields with different thresholds in different pixels. Threshold: the sum of Gaussian smoothing of Fig. 1a and a constant C.

• Fig. 1c, morphological closing operation and opening operation to remove small magnetic segments and get the ARs' kernel pixels, which are used as seeds in region growing.

• Fig. 1d, region growing to get all pixels of each single AR. All pixels connected to the seeds and stronger than the threshold are recovered.

• Fig. 1e, closing operation and removing decayed ARs segments that are smaller than an area threshold.

• Fig. 1f, merging neighbor regions and removing unipolar regions. Dilation operation to merge separate segments and multiply Fig. 1e to remove excess pixels. Drop all unipolar ARs whose flux imbalance is greater than 50%.

Calibration and Validation

To generate the homogenous ARs dataset for cycles 23 and 24, calibration between HMI and MDI data is required.

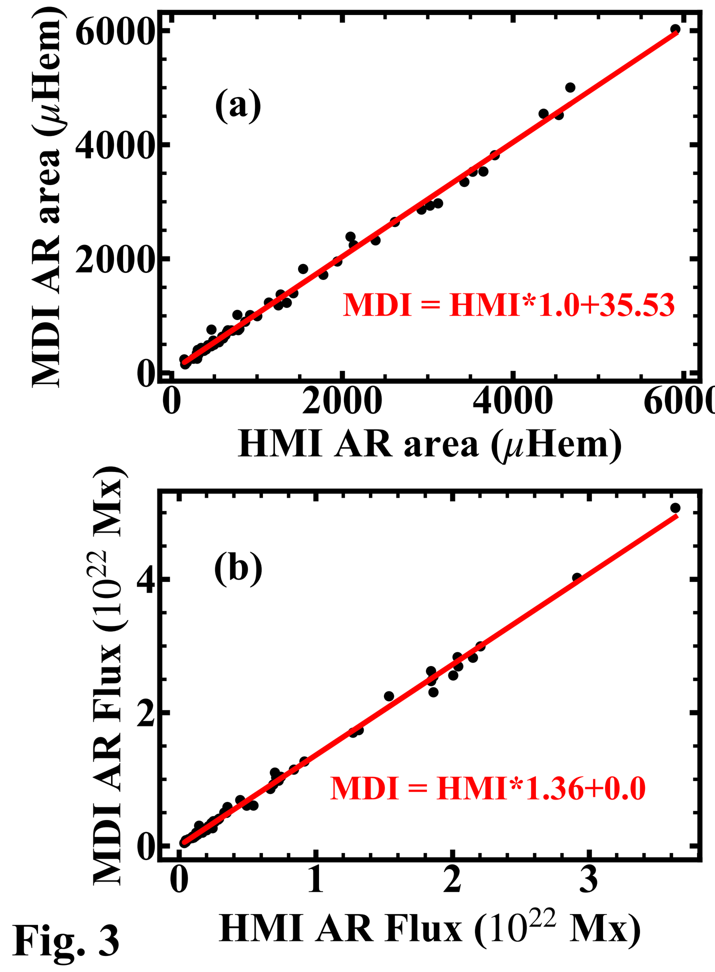

Fig. 3

Fig. 3. Calibration of the detected results based on MDI and HMI magnetograms. Top: scatter plot between MDI AR area and HMI AR area; Bottom: scatter plot between MDI AR flux and HMI AR flux. The red lines refer to linear functions that fit the data.

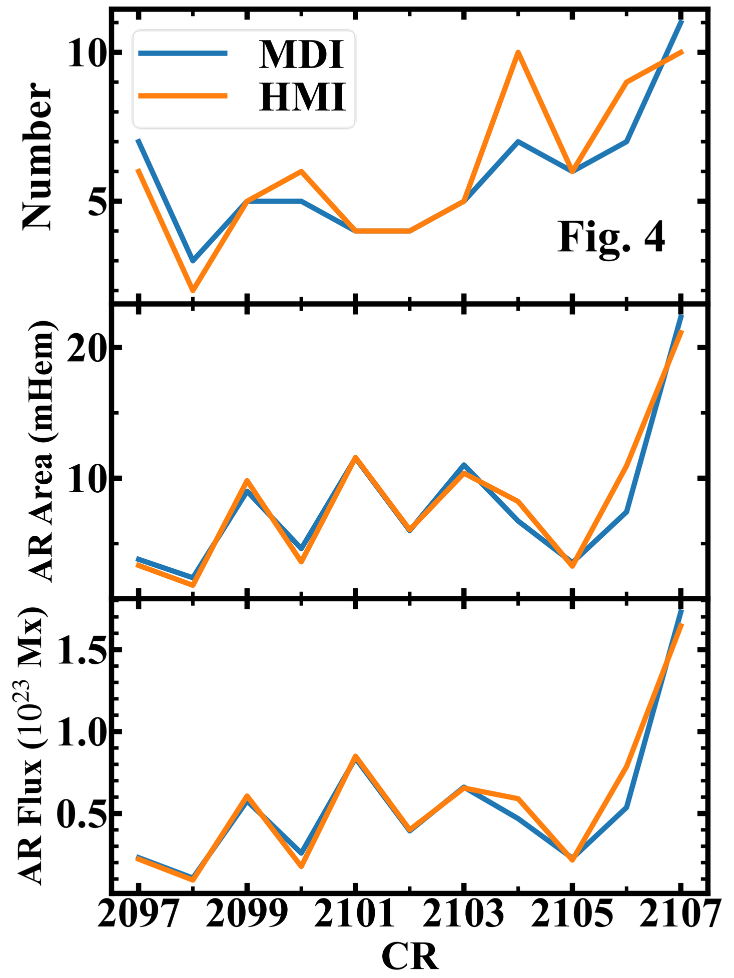

Fig. 4. Comparison of detected ARs during the 11 HMI and MDI overlap CRs. From top to bottom are the evolution of the detected ARs number, area, and flux. The latter two parameters are calibrated results.

Comparison with Other Datasets

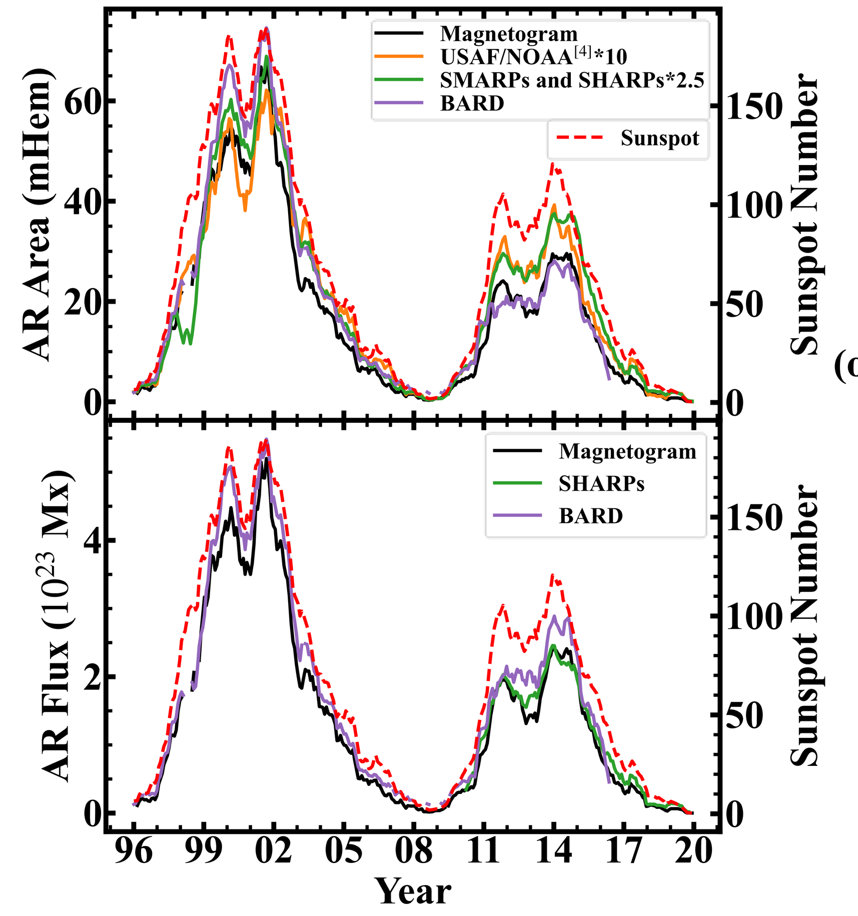

Fig. 5. Comparison of our results (black) with other datasets in the area (top) and flux (bottom). Sunspot number: red; USAF/NOAA sunspot area: orange; SMARPs and SHARPs (Bora et al., 2021, 2014): green; BARD (Munoz-Jaramillo et.al, 2016): pink.

Statistics of Different Strength ARs

• Strong ARs (blue): |flux| > 10^{22} Mx;
• Medium ARs (orange): 4×10^{21} Mx < |flux| < 10^{22} Mx;
• Weak ARs (green): |flux| < 4×10^{21} Mx.

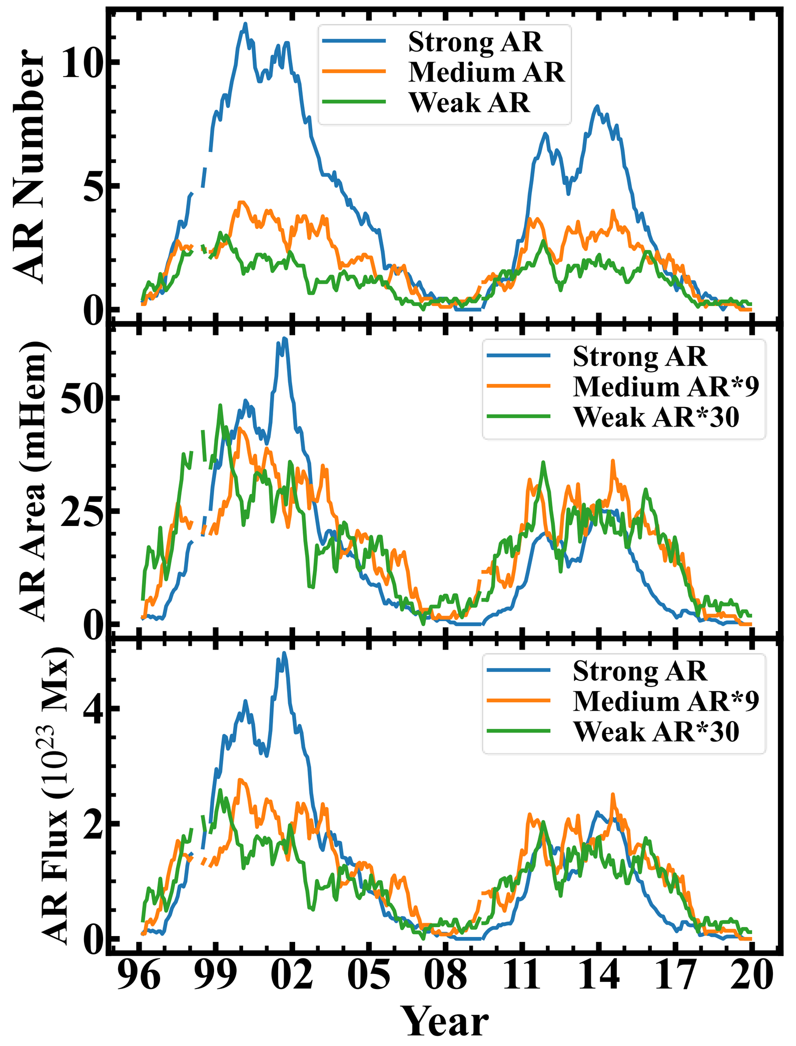

Fig.6. Statistical properties (Number: top; Area: middle; Flux: bottom) of the detected ARs in different strength of flux in cycles 23 and 24.